# Geometric Cloaks and Resonances

T. Curtright[§] and S. Subedi[∞]

Department of Physics, University of Miami, Coral Gables, FL 33124-8046, USA

[§]curtright@miami.edu [∞]sushil.subedi04@gmail.com

**Abstract**

Selected spatial geometries can either enhance or suppress scattering amplitudes, to produce either extremely sharp resonances or approximate invisibility for a specified angular momentum. A simple model is presented in detail for an impenetrable sphere surrounded by a Riemannian step geometry.

## Contents



## 1 Introduction

In principle, minimizing the total scattering cross-section of an object is one means to achieve its invisibility, at least partially [1]. For a circle embedded in 2 Euclidean dimensions (i.e. $S_1 \subset \mathbb{E}_2$), a 2-sphere embedded in 3 dimensions (i.e. $S_2 \subset \mathbb{E}_3$), or a hyper-sphere embedded in $N$ dimensions (i.e. $S_{N-1} \subset \mathbb{E}_N$), most often this minimization has been pursued previously by varying the potential within $S_{N-1}$ (or equivalently in the case of light, by varying the index of refraction). This minimization is pursued here by surrounding the hyper-sphere with non-trivial geometry [2] — that is to say, by dressing the hyper-sphere with a "Riemannian cloak" — but geometry sufficiently simple to permit exact analysis.

Alternatively, sharp resonances can be produced in the scattering cross-section by the same mechanisms. This is well-known for light (cf. Mie scattering [3]) and for potential scattering in quantum mechanics [4], but its implementation by geometric means is perhaps not so well-known.

Here we illustrate cloaking and resonances from geometric effects in the context of a simple model for a non-relativistic quantum particle scattering from an impenetrable circle/sphere/hyper-sphere surrounded by a Riemannian cloak in the form of a "geometric step." We give exact results only for the case of a sharp step, where the problem reduces to the implementation of some boundary conditions. For this case, we provide closed-form expressions for all the partial wave amplitudes which are valid for every $k$ in any number of spatial dimensions, but we give detailed plots and specific numerical results only for a small number of selected amplitudes and particular ranges of $kR$, especially for $N = 3$ ("3D").

## 2 Impenetrable hyper-spheres

Consider a plane wave in $N$ spatial dimensions incident on an impenetrable $S_{N-1}$ of radius $R$ for $N > 2$. For $r > R$ the partial wave expansion of the scattered wave function is[1]

$$\psi_{scattered}(r,\theta) = \sum_{\ell=0}^{\infty} (2\ell + N - 2)\, i^{\ell} \left(\frac{S_\ell - 1}{2}\right) {}_N\mathrm{h}_\ell^{(1)}(kr)\; {}_N\mathrm{P}_\ell(\cos\theta)$$

where our notation is defined in the Appendix, and we have assumed the dynamics is non-relativistic with $\hbar = 1 = m$, as well as $\left(\nabla^2 + k^2\right)\psi_{scattered} = 0$ for $r > R$. Demanding that $\psi(r,\theta) = \exp(ikr\cos\theta) + \psi_{scattered}(r,\theta)$ vanish at $r = R$ leads to the partial wave amplitudes

$$S_\ell = -\frac{{}_N\mathrm{h}_\ell^{(2)}(kR)}{{}_N\mathrm{h}_\ell^{(1)}(kR)} = -\frac{H^{(2)}_{\ell+\frac{N-2}{2}}(kR)}{H^{(1)}_{\ell+\frac{N-2}{2}}(kR)}$$

where the last expression is written in terms of the usual spherical Hankel functions, and is correct for $N \geq 2$. The angular-integrated partial wave cross-sections are then given by

$$\sigma_\ell = A_{\max}\, \frac{2(N-1)}{x^{N-1}} \frac{\Gamma(\ell + N - 2)}{\Gamma(\ell+1)} \frac{(2\ell + N - 2)\left(J_{\ell+(N-2)/2}(x)\right)^2}{\left(J_{\ell+(N-2)/2}(x)\right)^2 + \left(Y_{\ell+(N-2)/2}(x)\right)^2}$$

where $x \equiv kR$ and $A_{\max} = \frac{\pi^{\frac{N-1}{2}} R^{N-1}}{\Gamma\left(\frac{N+1}{2}\right)}$ is the cross-sectional hyper-area of the hyper-sphere as obtained from an equatorial slice. The total integrated cross-section is given by $\sigma_{total\,\ell} = \sum_{\ell=0}^{\infty} \sigma_\ell$ when $N > 2$.

We plot $\sigma_{total\,\ell}$ divided by $A_{\max}$, for various $N$, with $A_{\max}|_{N=2} = 2R$, $A_{\max}|_{N=3} = \pi R^2$, etc.

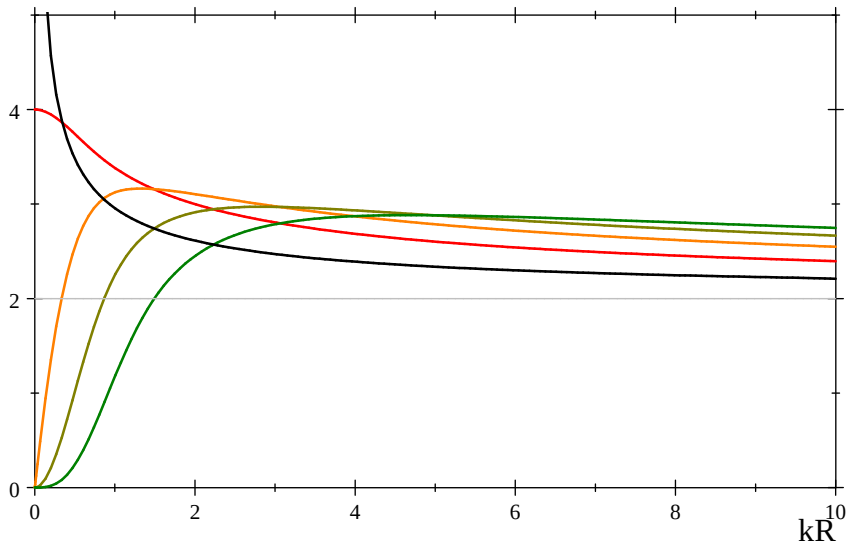


Impenetrable hyper-sphere $\sigma_{total}/A_{\max}$ versus $x = kR$ for $N = 2, 3, 4, 5,$ & $6$
in black, red, orange, brown, & green, respectively.

All of these total cross-sections vary smoothly with $kR$. There are no resonance spikes and no zeroes for $k > 0$, for any $N$. It is noteworthy, albeit expected, that $\lim_{k\to\infty} \sigma_{total\,\ell}/A_{\max} = 2$ for all $N$. On the other hand, the low momentum limit varies with $N$. For $N = 2$, $\lim_{k\to 0} \sigma_{total\,\ell} = \infty$, since $\sigma_0 \underset{k\to 0}{\sim} \frac{\pi^2}{k \ln^2(kR)}$. For $N = 3$, $\lim_{k\to 0} \sigma_{total\,\ell} = 4\pi R^2$, a fact which is often given the heuristic interpretation that the s-wave "feels" the entire surface area of the 2-sphere as $k \to 0$. This bogus explanation fails for other $N$, as evident from the fact that $\lim_{k\to 0} \sigma_{total\,\ell} \neq 2\pi R$ for $N = 2$. Moreover, $\lim_{k\to 0} \sigma_{total\,\ell} = 0$ for all $N > 3$.

[1] This expansion is written for $N > 2$. For $N = 2$ there is of course a similar expansion. The results to follow, for $S_\ell$, $\sigma_\ell$, and $\sigma_{total}$, are correct even in the limit $N \to 2$, provided both positive and negative integer $\ell$ are allowed for $N = 2$.

## 3 Riemannian step geometries

These are a class of Riemannian manifolds most easily envisioned for $N = 2$, where the two-dimensional metric of the manifolds may be defined by the embeddings [5]

$$(ds)^2 = (dr)^2 + r^2 (d\theta)^2 + (dz(r))^2 \quad , \quad z(r) = \frac{-\sqrt{2}H}{\sqrt{1 + \left(\frac{r}{R}\right)^{2M}}} \quad , \quad \text{with } r \geq R \text{ and } M \geq 0$$

Here $R$ and $H$ are constants, as is $M$, the latter being a class index for fixed $R$ and $H$. The dimensionless quantity $y = H/(2R)$ will be called the "aspect ratio" for the manifold. For the model to be considered, there is no need to continue the manifold to $r < R$ or to $z < -H$, since an impenetrable circular ring is envisioned at $(r, z) = (R, -H)$ with boundary condition $\psi = 0$ at that ring. Here are vertical profile plots of the embedded two-dimensional manifolds for various $M$.

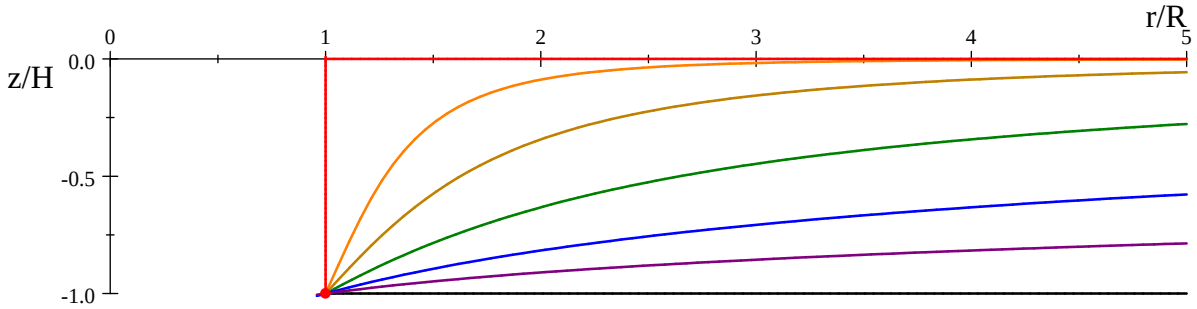


Riemannian step profiles embedded as $z(r) = \frac{-\sqrt{2}H}{\sqrt{1+\left(\frac{r}{R}\right)^{2M}}}$ for $r \geq R$ and plotted here for $M = 0, 1/4, 1/2, 1, 2, 4, \infty$ in black, purple, blue, green, sienna, orange, and red, respectively.

There are two especially tractable cases: $M = 0$, corresponding to a punctured plane with an impenetrable circular hole of radius $R$; and $M = \infty$, corresponding to a right circular cylinder of radius $R$ and height $H$ joined at one end to a punctured plane and terminated at the other end by an impenetrable circular ring.

Higher dimensional generalizations are less easily visualized, but have essentially the same structure, namely, a cylinder of height $H$ composed of hyper-spheres of radius $R$, joined at one end to a hyper-spherical hole in $\mathbb{E}_N$ and terminated at the other end by an impenetrable hyper-sphere again of radius $R$, where the metric of the manifolds may be defined by an embedding using standard spherical coordinates plus one additional $z(r)$ defined as above. That is to say,

$$(ds)^2 = (dr)^2 + r^2 (d\Omega_N)^2 + (dz(r))^2$$

Scattering for the $M = 0$ manifold is discussed in the previous section. In the rest of this paper we consider only the "sharp step" manifold obtained by taking $M \to \infty$, as pictured below for $N = 2$. Finite $M > 0$ will be discussed elsewhere [6].

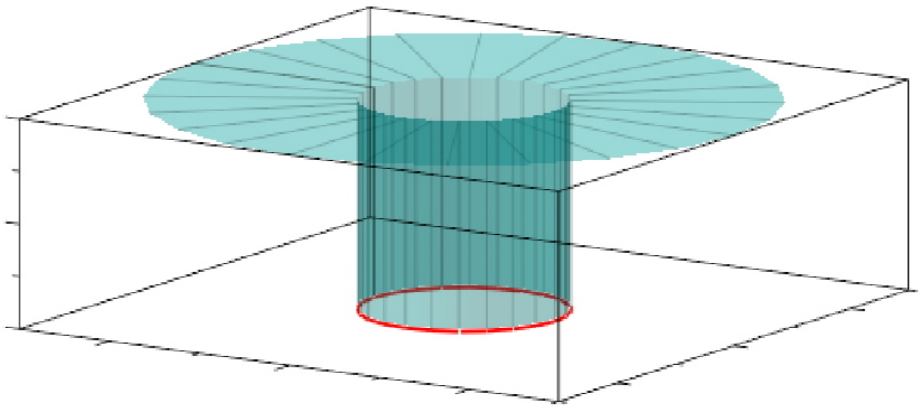

An impenetrable circle, in red, at the bottom of a circular cylinder attached to a punctured plane.

## 4 Partial wave amplitudes and cross-sections

For an impenetrable hyper-sphere of radius $R$ at the base of a hyper-spherical cylinder of height $H$, we require continuity of $\psi$ and its first derivatives at the edge that joins to $\mathbb{E}_N$, while the boundary condition we impose at the impenetrable edge of the hyper-cylinder is $\psi|_{\text{edge}} = 0$. This leads to [7]

$$S_\ell = -\left(\frac{\kappa R H^{(2)}_{\ell+\frac{N-2}{2}}(kR)\cos(\kappa H) + \left(kRH^{(2)}_{\ell+\frac{N}{2}}(kR) - \ell H^{(2)}_{\ell+\frac{N-2}{2}}(kR)\right)\sin(\kappa H)}{\kappa R H^{(1)}_{\ell+\frac{N-2}{2}}(kR)\cos(\kappa H) + \left(kRH^{(1)}_{\ell+\frac{N}{2}}(kR) - \ell H^{(1)}_{\ell+\frac{N-2}{2}}(kR)\right)\sin(\kappa H)}\right)$$

and thence to the amplitude for the scattered wave,

$$\begin{aligned} a_\ell(x,y,N) &\equiv i(1-S_\ell)/2 \\ &= i\left(\frac{\kappa R J_{\ell+\frac{N-2}{2}}(kR)\cos(\kappa H) + \left(kRJ_{\ell+\frac{N}{2}}(kR) - \ell J_{\ell+\frac{N-2}{2}}(kR)\right)\sin(\kappa H)}{\kappa R H^{(1)}_{\ell+\frac{N-2}{2}}(kR)\cos(\kappa H) + \left(kRH^{(1)}_{\ell+\frac{N}{2}}(kR) - \ell H^{(1)}_{\ell+\frac{N-2}{2}}(kR)\right)\sin(\kappa H)}\right) \end{aligned}$$

where $x \equiv kR$, $y \equiv H/(2R)$, $\kappa \equiv \sqrt{k^2 - \ell(\ell+N-2)/R^2}$, $\kappa R = \sqrt{x^2 - \ell(\ell+N-2)}$, and $\kappa H = 2y\kappa R = 2y\sqrt{x^2 - \ell(\ell+N-2)}$. In terms of these amplitudes the integrated partial wave cross-sections are given by

$$\sigma_\ell = A_{\max}(N)\ \frac{2\Gamma(N)}{x^{N-1}}\ \dim_\ell(N)\ \ |a_\ell(x,y,N)|^2$$

where $A_{\max}$ is again the maximum cross-sectional hyper-area, namely, $A_{\max}(N) = \frac{\pi^{\frac{N-1}{2}} R^{N-1}}{\Gamma\left(\frac{N+1}{2}\right)}$, and $\dim_\ell(N)$ is the dimension of a totally symmetric, irreducible $SO(N)$ tensor of rank $\ell$, namely, $\dim_\ell(N) = \frac{(2\ell+N-2)}{\Gamma(N-1)}\frac{\Gamma(\ell+N-2)}{\Gamma(\ell+1)}$. For the familiar $N = 3$ case, $A_{\max}(3) = \pi R^2$ and $\dim_\ell(3) = 2\ell+1$.

From the explicit expression for $S_\ell$ it follows that the scattering is elastic with $|S_\ell| = 1$ for *all* $k$ and *all* $\ell$ in *any* number of spatial dimensions, as should have been expected. Hence the complex amplitude $a_\ell(x,y,N)$ remains on the unitarity circle for all $k$. As examples, for $N = 3$ and aspect ratio $y = 2$, here are parametric Argand plots of $(\text{Re}\, a_\ell(x), \text{Im}\, a_\ell(x))$ for $\ell = 0$ & 1, with selected values of $x$ shown as dots arrayed counterclockwise from the origin. These plots are indicative of sharp resonances, with $a_\ell$ moving rapidly counterclockwise through the top of the unitarity circle as $x \equiv kR$ changes through a small interval.

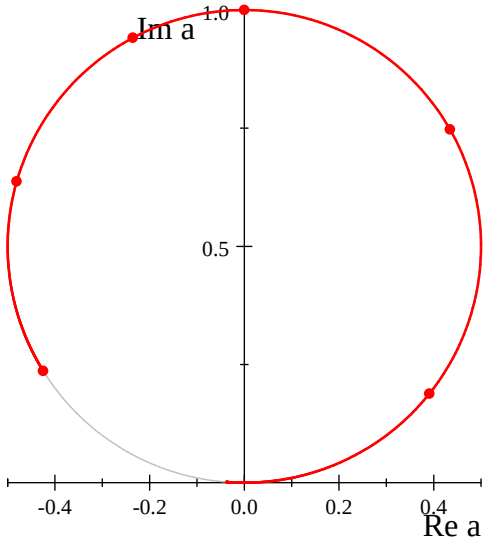


3D $(\text{Re}\, a_0, \text{Im}\, a_0)$ for $y = 2$ & $0 \le x \le 1$ with $x = 0.6,\ 0.65,\ 0.682,\ 0.7,\ 0.75,$ & 1 shown as dots.

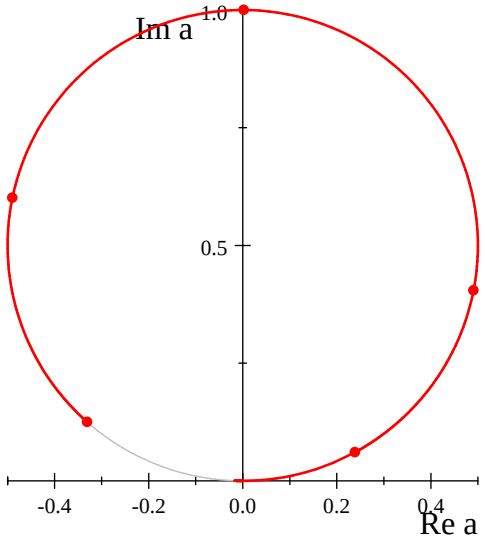


3D $(\text{Re}\, a_1, \text{Im}\, a_1)$ for $y = 2$ & $0 \le x \le 1.65$ with $x = 1.5,\ 1.55,\ 1.5786,\ 1.6,$ & 1.65 shown as dots.

## 5 Resonance reconnaissance

Consider three-dimensional scattering for two illustrative aspect ratios, $y = H/(2R)$. First, consider $y = 1$ for $0 \leq kR \leq 5$.

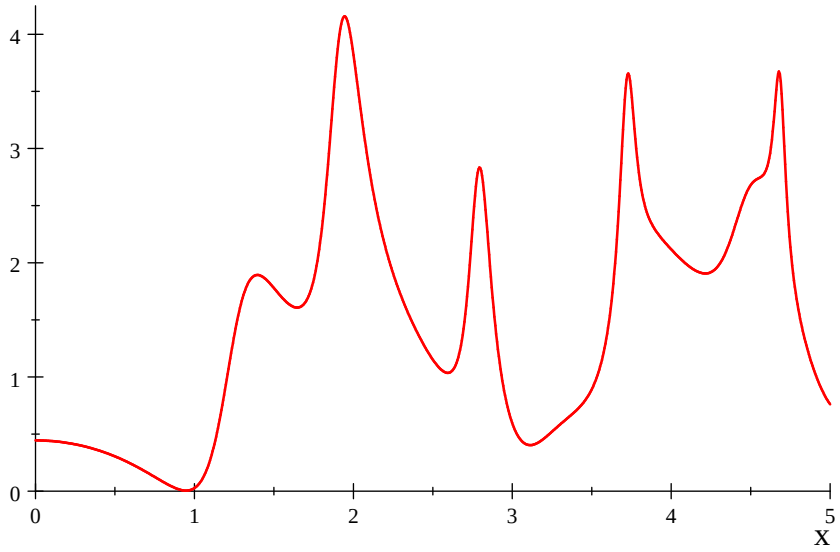


3D $\sigma_{total}/\left(\pi R^2\right)$ versus $x = kR$ for aspect ratio $y = 1$.

There are four sharp resonances clearly visible in $\sigma_{total\ell}$, corresponding to angular momenta $\ell = 1, 2, 3, 4$ as evident in the $\sigma_\ell$ partial cross-sections, plotted here with the unitarity bounds shown as light gray curves.

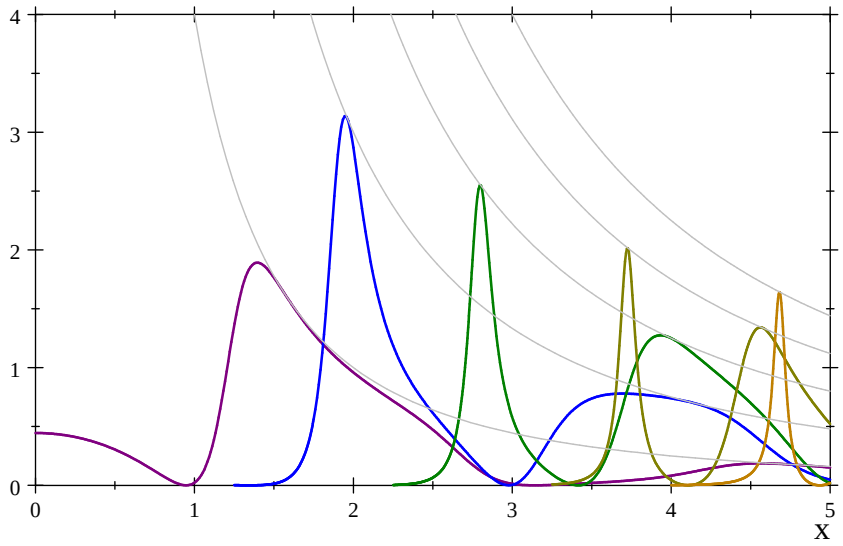


3D $\frac{1}{\pi R^2}\ \sigma_\ell\,(x, y = 1)$ for $\ell = 0, 1, 2, 3, 4$ in purple, blue, green, brown, and sienna, respectively.

Consistent with the general principles of potential scattering [4] these four sharp peaks, as well as successive narrow resonances at higher values of $\ell$, correspond to lower half-plane complex $k$ or $w = kR$ poles in the various scattering amplitudes. For large $\ell$ the real parts increase approximately linearly, $\mathrm{Re}\, w_\ell \approx \ell + 1/2$. Numerically:

$$w_{\ell=1} = 1.9076 - 0.13812i,\quad w_{\ell=2} = 2.7863 - 0.089056i,\quad w_{\ell=3} = 3.7228 - 0.06298i,\quad w_{\ell=4} = 4.6831 - 0.047383i$$
$$w_{\ell=5} = 5.6558 - 0.03721i,\quad w_{\ell=6} = 6.6357 - 0.030158i,\quad w_{\ell=7} = 7.6203 - 0.02504i,\quad w_{\ell=8} = 8.6081 - 0.021194i$$

Note that the imaginary parts of these poles, i.e. the widths of the narrow resonances, decrease in magnitude as $\ell$ increases, approximately as $\ell^{-3/2}$ for large $\ell$. Also note the asymmetrical shape of the broader peaks suggests they are Fano resonances.

Next, consider $y = 2$, again for $0 \leq kR \leq 5$. There are now about twice as many narrow resonances as there were for $y = 1$, if not more, again as evident in $\sigma_{total\ell}$.

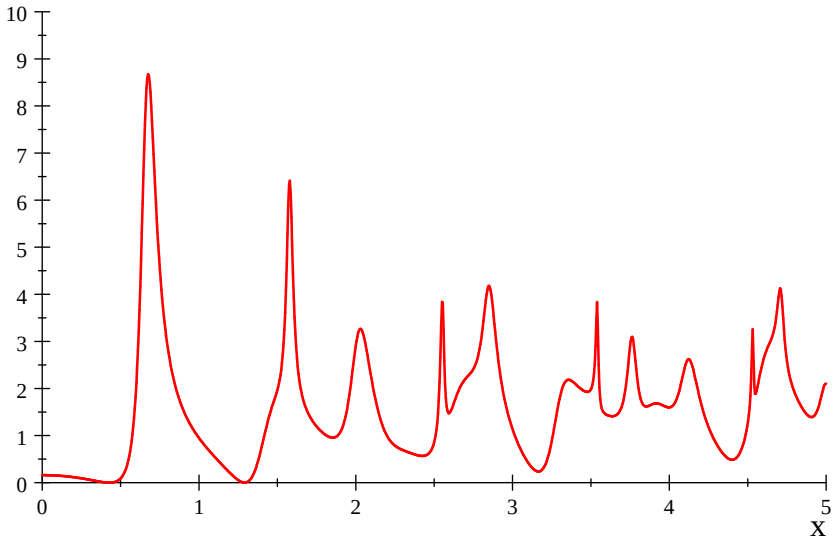


3D $\sigma_{total}/\left(\pi R^2\right)$ versus $x = kR$ for aspect ratio $y = 2$.

In this case there is also a strong $\ell = 0$ resonance, as well as narrow peaks occurring in pairs for each value of $\ell = 1, 2, 3, 4$, albeit with discernibly different widths, as is evident from plots of the various $\sigma_\ell$ partial cross-sections. The resonance peaks again reach the unitarity bounds (light gray curves) for all $\ell$.

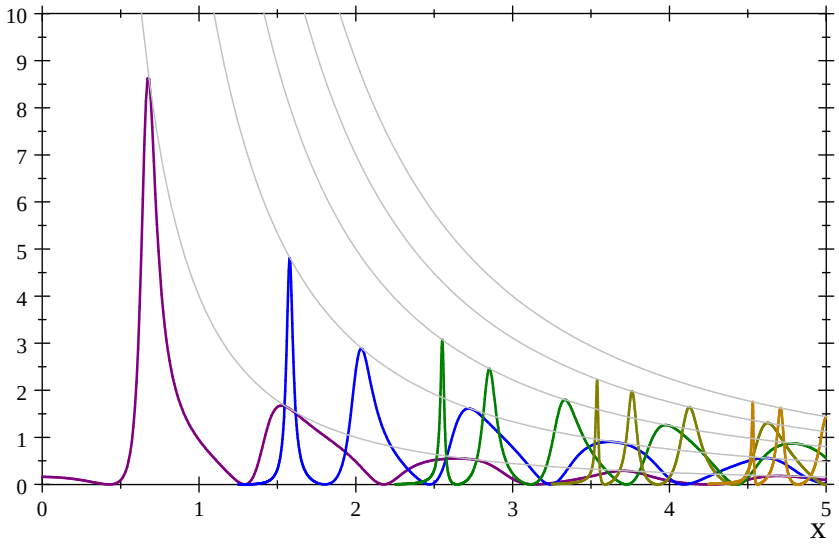


3D $\frac{1}{\pi R^2}\ \sigma_\ell\,(x, y = 2)$ for $\ell = 0, 1, 2, 3, 4$ in purple, blue, green, brown, and sienna, respectively.

As before, these $y = 2$ resonances correspond to lower half-plane complex $k$ or $w = kR$ poles in the various scattering amplitudes, with real parts spaced approximately linearly in $\ell$, and once again the corresponding resonance widths tend to decrease approximately as $\ell^{-3/2}$ for large $\ell$. Numerically:

$$w_{\ell=0} = 0.662563 - 0.0581809i\ , \qquad w_{\ell=1} = 1.57735 - 0.0253699i\ \&\ 2.01 - 0.0844143i\ ,$$
$$w_{\ell=2} = 2.5527 - 0.0148254i\ \&\ 2.84723 - 0.054063i\ \&\ 3.29479 - 0.104328i$$
$$w_{\ell=3} = 3.54032 - 0.00993167i\ \&\ 3.76278 - 0.0375217i\ \&\ 4.11432 - 0.0766773i$$
$$w_{\ell=4} = 4.53275 - 0.00720854i\ \&\ 4.71142 - 0.027726i\ \&\ 4.99907 - 0.0583968i\ \&\ 5.38212 - 0.0947985i$$

Here we have displayed additional poles for $\ell = 2,\ 3,\ \&\ 4$ whose resonance widths are comparable to those shown for $\ell = 0\ \&\ 1$. The asymmetrical shape of the broader peaks again suggests they are Fano resonances.

## 6 Hide and seek

The $k \to 0$ limit of the cross-section varies markedly with the aspect ratio $y$. In 3D it is

$$\lim_{k\to 0} \sigma_{total\ell}|_{N=3} = \lim_{x\to 0} \sigma_0\,(x,y)|_{N=3} = 4\pi R^2/\,(1+2y)^2$$

This would suggest that larger values of $y$ would suppress the low momentum cross-section and tend to make the system "stealthy" for small $k$, although not completely invisible [7]. However, it is also true that $\sigma_{total\ell}$ exhibits resonances for larger $y$ and the lowest momentum resonance occurs in $\sigma_0$ for $x$ that decreases as $y$ increases. Thus there is a trade-off between the two effects: Low momentum scattering is reduced but only for a range of $k$ going from zero up to the appearance of the first resonance. These features are exhibited in the following two Figures.

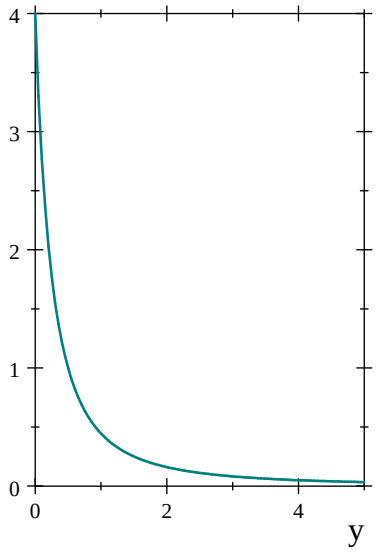


3D $\lim_{k\to 0} \sigma_{total}/\left(\pi R^2\right)$ versus the aspect ratio $y$.

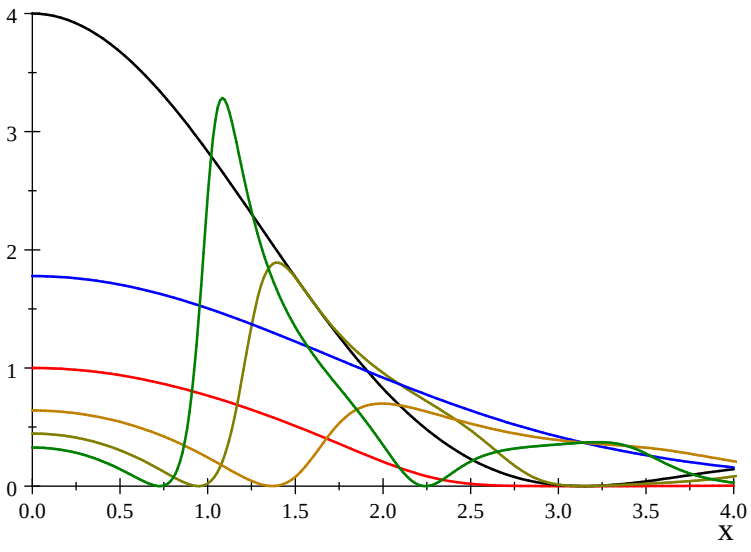


3D $\sigma_0/\left(\pi R^2\right)$ for $y = 0,\ 1/4,\ 1/2,\ 3/4,\ 1,$ & $5/4$ in black, blue, red, sienna, brown, & green, respectively.

Of course, higher $\ell$ partial waves also contribute to $\sigma_{total\ell}$ as $x$ increases, and these must be taken into account to determine how effectively the geometric cloak has prevented the impenetrable sphere from scattering the incident plane waves. This is shown here:

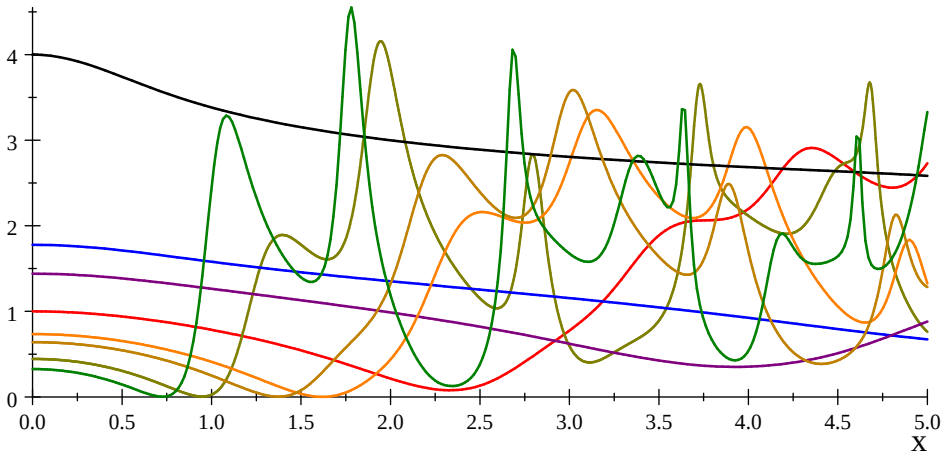


3D $\sigma_{total}/\left(\pi R^2\right)$ versus $x = kR$ for aspect ratios $y = 0,\ 1/4,\ 1/3,\ 1/2,\ 2/3,\ 3/4,\ 1,$ & $5/4$ in black, blue, purple, red, orange, sienna, brown, & green, respectively.

While scattering a wave packet consisting of only low momenta would be more precise, a rough criterion for the invisibility of the system would be to compute the cross-section for an incoherent sum of various $k$ plane waves, say from zero up to $k_{\max} = \pi/R$, corresponding to a wavelength equal to the diameter of the sphere, $\lambda = 2R$. This is easily done numerically. For example, for $y = 1/2$:

$$\frac{1}{\pi R^2} \sum_{\ell=0}^{3} \int_0^{\pi} \sigma_\ell\,(x)\,dx \Bigg|_{N=3} = 1.849$$

That is to say, $y = 1/2$ gives a very good estimate for the minimum of this incoherent sum (the same sum for $y = .49$ is $1.858$ while for $y = 0.51$ the sum is $1.854$). In this sense when $y = 1/2$ the system is least visible to low momentum incident waves.

There is a simple plausibility argument why this should be so. If the aspect ratio is $y = 1/2$ then $H = R$. The condition $\psi = 0$ at the impenetrable cylinder edge mimics the effect of $\psi = 0$ at $r = 0$ for an *un*cloaked and *un*punctured space. Naively then, from a path integral perspective, it would seem that the phase acquired along a particle path crossing the cylinder for $H = R$ would be the same as the phase acquired by a free particle propagating radially on an uncloaked and unpunctured $\mathbb{E}_3$ from $r = R$ to $r = 0$. Hence, naively, the net effect of the combined cylinder and impenetrable sphere for $H = R$ would be the same as no scattering center whatsoever. Moreover, this plausibility argument would seem to apply just as well for $N > 3$.

On the other hand, such plausibility arguments are no substitute for exact calculations. Indeed, numerically for $N = 5$, say, this same incoherent cross-section sum has a minimum for $y \approx 0.43$ rather than $y = 1/2$. (Close, but no cigar! The disparity seems to be due to a broad s-wave resonance lying below $kR = \pi$ for $N = 5$ and $y \approx 1/2$. See the following Figure.) Nevertheless, the heuristics here seem to hold up better for $N \neq 3$ than the bogus "total surface area" estimate for $\lim_{x\to 0} \sigma_{total\,\ell}$ in the case of an uncloaked impenetrable sphere.

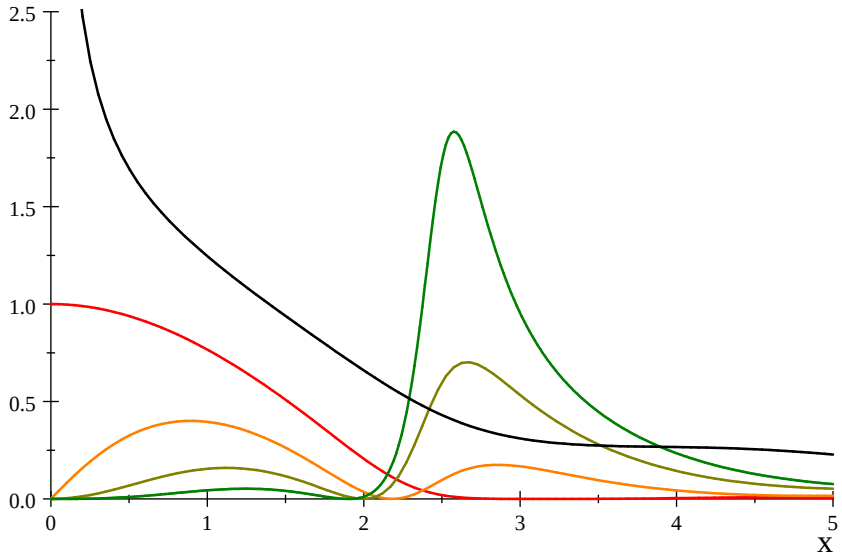


$\sigma_0/A_{\max}$ for $y = 1/2$ and $N = 2,\ 3,\ 4,\ 5,$ & $6$
in black, red, orange, brown, & green.

# 7 Conclusions

Our analysis of the simple cloaked sphere geometric model has shown that resonances are produced more prodigiously as $y$ increases, an effect somewhat similar to what happens in Mie scattering when the index of refraction is increased [3]. Moreover, if the geometry is complexified by continuation of $y$ into the complex plane, inelastic scattering effects appear [6], which is again somewhat similar to complex refraction index effects. In any case such resonances tend to make it more difficult for the model to achieve stealth and invisibility to low momentum incident waves.

Since our analysis has been non-relativistic, we believe it may be useful as written for understanding suitably designed, nanoscale quantum devices [8], devices that it might be possibe to fabricate in the laboratory, say for $N = 2$. However, we also believe most of the interesting features can be found in relativistic models where time is not universal, say in the context of general relativity, but this remains to be fully pursued, especially in higher dimensional spacetimes.

**Acknowledgements** We thank O. Korotkova for pointing out the review article by G. Gbur [1].

# Appendix: Spherical functions

Following Sommerfeld's lead [9] (modulo a bit of typesetting to avoid the standard notation of Jacobi polynomials) a convenient notation for "hyper-spherical polynomials" in $N > 2$ spatial dimensions would be

$$ {}_{N}\mathrm{P}_{\ell}(x) \equiv C_{\ell}^{\left(\frac{N-2}{2}\right)}(x) \tag{A1} $$

where $C_{\ell}^{(\alpha)}$ are Gegenbauer polynomials, and a corresponding notation for "hyper-spherical Bessel functions" would be

$$ {}_{N}\mathrm{j}_{\ell}(s) \equiv \frac{1}{2\,(s/2)^{\frac{N-2}{2}}}\,\Gamma\left(\tfrac{N-2}{2}\right) J_{\ell+\frac{N-2}{2}}(s)\ , \quad {}_{N}\mathrm{y}_{\ell}(s) \equiv \frac{1}{2\,(s/2)^{\frac{N-2}{2}}}\,\Gamma\left(\tfrac{N-2}{2}\right) Y_{\ell+\frac{N-2}{2}}(s)\ , \tag{A2} $$

$$ {}_{N}\mathrm{h}_{\ell}^{(1,2)}(s) \equiv {}_{N}\mathrm{j}_{\ell}(s) \pm i\ {}_{N}\mathrm{y}_{\ell}(s) = \frac{1}{2\,(s/2)^{\frac{N-2}{2}}}\,\Gamma\left(\tfrac{N-2}{2}\right) H^{(1,2)}_{\ell+\frac{N-2}{2}}(s) \tag{A3} $$

where $J_\nu$, $Y_\nu$, and $H_\nu^{(1,2)} = J_\nu \pm iY_\nu$ are the usual Bessel and Hankel functions. In terms of these the expansion of a plane wave in $N > 2$ dimensions is expressed uniformly as

$$ e^{ikr\cos\theta} = \sum_{\ell=0}^{\infty} (2\ell + N - 2)\, i^{\ell}\ {}_{N}\mathrm{j}_{\ell}(kr)\ {}_{N}\mathrm{P}_{\ell}(\cos\theta) \tag{A4} $$

(As is well-known, for $N = 2$ a similar expansion holds provided negative integer $\ell$ are included.) These hyper-spherical Bessel functions obey the same first order recursion relations for all $N$, namely,

$$ s\ \frac{d}{ds}\ {}_{N}\mathrm{j}_{\ell}(s) = \ell\ {}_{N}\mathrm{j}_{\ell}(s) - s\ {}_{N}\mathrm{j}_{\ell+1}(s) \tag{A5} $$

Similarly for ${}_{N}\mathrm{y}_{\ell}(s)$ and ${}_{N}\mathrm{h}_{\ell}^{(1,2)}(s)$. Also note the $N$-dependent Wronskian,

$$ W\left[{}_{N}\mathrm{h}_{\ell}^{(1)}(s)\,,\,{}_{N}\mathrm{h}_{\ell}^{(2)}(s)\right] = \frac{1}{(s/2)^{N-2}}\,\Gamma^2\left(\tfrac{N-2}{2}\right)\left(\frac{1}{i\pi s}\right) \tag{A6} $$

where $W[f, g] = fg' - f'g$.

The partial wave expansion of the scattering amplitude is obtained by modifying the radially outgoing component[2] of the plane wave in (A4), i.e. by writing

$$ \psi(r,\theta) = \sum_{\ell=0}^{\infty} (2\ell + N - 2)\, i^{\ell}\left(\frac{S_\ell}{2}\ {}_{N}\mathrm{h}_{\ell}^{(1)}(kr) + \frac{1}{2}\ {}_{N}\mathrm{h}_{\ell}^{(2)}(kr)\right) {}_{N}\mathrm{P}_{\ell}(\cos\theta) \tag{A7} $$

for points outside a localized scattering center. This expansion supposes the scatterer is invariant under all rotations that preserve the direction of the incoming plane wave, such that $\psi$ does not depend on the other $N - 2$ spherical coordinate angles.

[2] Time dependence is understood to be given by the usual convention in non-relativistic quantum mechanics, namely, $\exp(-iEt)$ with $E = k^2$. This is not always the case in the optics literature, where the time dependence is often taken to be $\exp(+i\omega t)$. For example, see [3].

# References


[1] G. Gbur, "Invisibility Physics: Past, Present, and Future" Progress in Optics 58 (2013) 65-114.

[2] U Leonhardt and T Philbin, *Geometry and light: The science of invisibility*, Dover (2010).

[3] H C van de Hulst, *Light Scattering by Small Particles*, Dover (1981).

[4] R G Newton, *Scattering Theory of Waves and Particles*, 2nd Edition, Dover (2013).

[5] For $M = 1$ this is a static limit for the "upper half" of an Ellis wormhole. See H.G. Ellis, "Ether flow through a drainhole: A particle model in general relativity" J. Math. Phys. 14 (1973) 104–118.

[6] T L Curtright and S Subedi, "Holistic Scattering" *in preparation.*

[7] Note that $\kappa$ depends on the partial wave number $\ell$ as well as $k$, and that $S_\ell$ is identical to that of the uncloaked impenetrable sphere whenever $\kappa H = m\pi$.

[8] Jeng Yi Lee and Ray-Kuang Lee, "Hide the interior region of core-shell nanoparticles with quantum invisible cloaks" https://arxiv.org/abs/1306.2120.

[9] A Sommerfeld, *Partial Differential Equations in Physics*, Academic Press (1964).